

# Two-stage approach for the inference of the source of high-dimension and complex chemical data in forensic science

M.A. Ausdemore, M.Sc.\*  
and  
C. Neumann, Ph.D.  
and  
C.P. Saunders, Ph.D.  
and  
D.E. Armstrong, Ph.D.

Department of Mathematics and Statistics,  
South Dakota State University, Brookings, U.S.A.

May 18, 2022

## Abstract

While scholars advocate the use of a Bayes factor to quantify the weight of forensic evidence, it is often impossible to assign the necessary probability measures for high-dimension and complex data, and so performing likelihood-based inference is impossible. We address this problem by leveraging the properties of kernel functions to propose an inference framework based on a two-stage approach to offer a method that allows to statistically support the inference of the identity of source of trace and control objects. Our method is generic and can be tailored to any type of data encountered in forensic science or pattern recognition.

*Keywords:* Bayesian inference, likelihood-based inference, kernel-based methods,

technometrics tex template (do not remove)

---

\*The authors gratefully acknowledge Dr. Cyril Muehlethaler from the Université du Québec à Trois Rivières, Canada, for his data. This project was supported in part by Award No. 2014-IJ-CX-K088 awarded by the National Institute of Justice, Office of Justice Programs, U.S. Department of Justice. The opinions, findings, and conclusions or recommendations expressed in this paper are those of the authors and do not necessarily reflect those of the Department of Justice.

# 1 Introduction

Given  $M$  trace objects assumed to originate from a single source, and  $N$  control objects from a known source, we want to help decide if all  $N + M$  objects originate from the same source. Formally, we want to test if:

$H_1$  - the  $M$  trace and  $N$  control objects are two simple random samples from the source of the  $N$  control objects;

$H_2$  - the  $M$  trace objects is a simple random sample from another source in a population of potential sources.

In forensic science, differentiating between these two propositions cannot be reduced down to a simple classification or model selection problem that can be directly addressed by machine learning or other similar techniques. Indeed, as we will explain below, the inference process needs to account for the many sources in the population that are potentially indistinguishable from the source of the  $N$  control objects. Thus, legal and scientific scholars advocate the use of a Bayes factor to quantify the support of the observations made on the trace and control objects in favour of one of these two propositions (see Aitken et al. (2010) for a comprehensive discussion).

Unfortunately, it is often impossible to assign probability measures to the high-dimension and complex data commonly encountered in forensic science. For example, the random vectors associated with the chemical spectra characterising glass, paint, fibre or dust evidence may have thousands of dimensions and include different types of data (e.g., discrete, continuous, compositional). Without these probability measures, assigning Bayes factors, or performing any other likelihood-based inference, is not possible.

In this paper, we propose to revisit the *two-stage approach* formally introduced by Parker (1966, 1967) in the light of new developments in statistical pattern recognition and the availability of modern computational systems. In particular, we leverage the properties of kernel functions (Schoelkopf and Smola, 2001) and the results presented by Armstrong et al. (2017) to propose a generic inference framework that can be tailored to any type of data encountered in forensic science, and in particular to evidence types characterised by their chemical compositions. Despite the shortcomings discussed later in this paper, we believe

that the two-stage approach can provide a helpful and rigorous statistical framework to support the inference of the identity of source of trace and control objects described by high-dimension heterogeneous random vectors.

## 2 Overview of the two-stage approach

The general framework of the two-stage approach was first briefly mentioned by Kingston 1965 and formally described by Parker (1966, 1967). Parker breaks down the forensic inference process into two stages, which he describes as the *similarity stage*, and the *identification stage*. In the similarity stage, the goal is to compare the characteristics of the trace and control objects and determine whether they are *distinguishable*. As the difference between the sets of characteristics increases, the hypothesis that the trace and control objects originate from the same source is weakened to the point that it can be rejected. However, establishing that the two sets of characteristics are indistinguishable is not sufficient in itself to conclude to the identity of the source of the two sets of objects. Intuitively, the value of finding that the set of characteristics of the trace objects are indistinguishable from those of the control objects is a function of the number of sources whose characteristics would also be deemed indistinguishable from the trace objects using the same analytical technique: the lack of distinguishability between trace and control objects is more valuable in cases where very few sources in a population of potential sources share the same characteristics as the trace objects. For example, the information that the type of the blood recovered at a crime scene is the same as the one of a suspect will be a lot more helpful to support the inference that the blood comes from the suspect if the blood type is AB<sup>-</sup> (less than 1% of the population) than if the blood type is O<sup>+</sup> (approx. 40% of the population). Thus, the goal of the identification stage is to determine the rarity of the characteristics observed in the first stage in the population of potential sources. The level of rarity of the trace characteristics in a population of potential sources is often called a *match probability* or *probability of coincidence*.

While occasional early uses of Bayesian inference in the judicial system have been reported (Taroni et al., 1999), the two-stage approach appears to be an initial attempt to formally frame the problem of the inference of the identity of source in forensic science in

a logical manner, and to propose a statistically rigorous method to support this inference process. Today, the two-stage approach naturally arises as a proxy for the Bayes factor in situations where the measurements made on the trace and control objects are discrete and can easily be compared, such as in single-source forensic DNA profiling: the DNA profile of a trace and of a known individual are compared, and if found similar, the match probability of that profile in a population of potential donors is determined (Butler, 2015).

The two-stage approach was refined in the context of glass evidence by Evett in a series of papers starting in 1977 (Evett, 1977). Today, ad-hoc implementations of the two-stage approach can notably be found in relation to glass, paint and fibre evidence. In most cases, the decision to reject the hypothesis that trace and control objects are indistinguishable during the first stage is based on the *training* and *experience* of the forensic analyst performing the examination; the determination of the match probability during the second stage relies, in the best situation, on frequency estimates obtained by determining the size of an ill-defined set of objects that are considered to have the “same characteristics” as those of the trace (Kaye, 2017). Outside of trivial situations with discrete data (e.g., blood typing) or low dimension continuous data (e.g., refractive index of glass), we have not found a rigorous implementation of the two-stage approach that could handle high-dimension and complex forms of evidence, such as chemical spectra, and impression and pattern evidence, and we have to agree with the arguments brought forward by Kaye (2017).

Below, we propose a formal statistical method to test the hypothesis that two high-dimension and complex sets of observations are indistinguishable (Parker’s similarity stage). We extend the work published by Armstrong et al. (2017) to develop a generic  $\alpha$ -level test to compare high-dimension heterogenous random vectors, in which we account for the uncertainty on the model’s parameters, and we propose a computationally efficient algorithm that enables to increase the number of objects considered and to improve the reliability of the test. Because our test relies on kernel functions that can be tailored to any type of data, the same test can be used in multiple situations, irrespectively of the type of evidence considered.

Our method improves upon existing pattern recognition methods that could be consid-

ered to address this type of problems, such as Support Vector Machines, Artificial Neural Networks, or Random Forests, in the sense that our method does not require a training set, allows for likelihood-based inference, and enables formal statistical hypothesis testing in high-dimension.

In this paper, we present strategies to assess the performance of the statistical test and we explore the extension of the method to the second stage (Parker’s identification stage). Finally, we discuss the benefits and limitations of the two-stage approach in the context of the inference of the source of high-dimension complex forms of forensic evidence.

### 3 First stage: testing *indistinguishability*

In the first stage of our approach, we wish to test whether the  $M$  trace objects are indistinguishable from the  $N$  control objects. We use an  $\alpha$ -level test to address  $H_1$  and  $H_2$ . Given the nature on the test, we can only reach one of two conclusions:

1.  $H_2$  is true, the trace and control objects are different and they do not originate from the same source;
2. We do not have enough evidence to reject the possibility that the trace and control objects originate from the same source, and we fail to reject  $H_1$  at the chosen  $\alpha$ -level.

We want to reiterate that, in the forensic context, the latter conclusion does not directly imply that the trace and control objects originate from the same source: it merely implies that the sources of the trace and control objects are indistinguishable from each other, based on the considered characteristics and the chosen  $\alpha$ -level. As mentioned above, the value of finding that these sources are indistinguishable can be assessed only in the light of the number of sources that would also be found indistinguishable. Assessing the rarity of the trace’s characteristics is the purpose of the second of the two stages of the approach and is addressed later in this paper.

To statistically test  $H_1$  and  $H_2$  in presence of high-dimension, heterogenous and complex data, we use the methodology sketched in O’Brien (2017). We extend the results presented by Armstrong et al. (2017) and reported in Appendix I to develop a statistical test using vectors of scores resulting from the cross-comparison of the trace and control objects.

### 3.1 $\alpha$ -level test for vectors of scores

Given two vectors of measurements  $\mathbf{x}_i$  and  $\mathbf{x}_j$  representing the observations made on two objects,  $i, j$ , sampled from a common source, a kernel function,  $\kappa$ , is used to measure their level of similarity and report it as a score,  $s_{i,j}$ .

$$s_{i,j} = \kappa(\mathbf{x}_i, \mathbf{x}_j) \quad (1)$$

We note that the kernel function at the core of the model,  $\kappa$ , can be designed to accommodate virtually any type of data. It needs satisfy only two requirements: it must be a symmetric function, that is  $\kappa(\mathbf{x}_i, \mathbf{x}_j) = \kappa(\mathbf{x}_j, \mathbf{x}_i)$ ; and it must ensure that the marginal distribution of  $s_{ij}$  is normal to satisfy the assumption made on the score model by Armstrong et al. (2017) when developing their model. This assumption is reasonable for high-dimension objects and can be satisfied through careful design of the kernel function (Armstrong, 2017).

Given  $M$  trace and  $N$  control objects, we define the vector of scores  $\mathbf{s}_{m+n} = \begin{pmatrix} \mathbf{s}_m \\ \mathbf{s}_n \end{pmatrix}$ , where  $\mathbf{s}_n$  represents the  $n = \binom{N}{2}$  scores calculated between all pairs of control objects, and  $\mathbf{s}_m$  represents the  $m = \binom{N+M}{2} - \binom{N}{2}$  scores calculated between all pairs of objects involving at least one of the trace objects.

Since all control objects are known to originate from a single source, we use the results in Armstrong et al. (2017) to assume  $\mathbf{s}_n \sim MVN(\theta \mathbf{1}_n, \Sigma_{n \times n})$  with  $\Sigma_{n \times n} = \mathbf{P} \mathbf{P}^t \sigma_a^2 + \mathbf{I}_n \sigma_e^2$ , and parameter  $\Psi = \{\theta, \sigma_a^2, \sigma_e^2\}$ , where  $\theta$  is the expected value of the score between any two objects from the same considered source,  $\sigma_a^2$  and  $\sigma_e^2$  are the variances of two random effects, and  $\mathbf{P}$  is an  $n \times N$  design matrix where each row represents an  $i, j$  combination of objects and consists of ones in the  $i^{th}$  and  $j^{th}$  columns and zeros elsewhere.

Furthermore, under  $H_1$ , all trace and control objects are assumed to originate from the same source, therefore

$$\begin{aligned} \begin{pmatrix} \mathbf{s}_m \\ \mathbf{s}_n \end{pmatrix} | H_1 &\sim MVN(\theta \mathbf{1}_{(m+n)}, \Sigma_{(m+n) \times (m+n)}) \\ &= MVN\left(\theta \mathbf{1}_{(m+n)}, \begin{bmatrix} \Sigma_{m \times m} & \Sigma_{m \times n} \\ \Sigma_{n \times n} & \Sigma_{n \times m} \end{bmatrix}\right) \\ &= MVN(\theta \mathbf{1}_{(m+n)}, \mathbf{Q} \mathbf{Q}^t \sigma_a^2 + \mathbf{I}_n \sigma_e^2) \end{aligned} \quad (2)$$

where  $\mathbf{Q}$  is a design matrix similar to  $\mathbf{P}$  with the appropriate dimensions. Under  $H_1$ , this

distribution has the same parameter,  $\Psi = \{\theta, \sigma_a^2, \sigma_e^2\}$ , as the distribution of  $\mathbf{s}_n$ , since the only difference between them are the length of the mean vector and the dimensions of the design matrices  $\mathbf{P}$  and  $\mathbf{Q}$ .

We begin designing the test statistic of our  $\alpha$ -level test by defining the *conditional likelihood* of the vector of scores involving at least one trace object, given the vector of scores involving only control objects,  $\mathcal{L}(\mathbf{s}_m|\mathbf{s}_n, \Psi)$ . Then we define our test statistic as the function

$$T(\mathbf{s}_m, \mathbf{s}_n, \Psi) = \Pr(\mathcal{L}(\mathbf{s}_m|\mathbf{s}_n, \Psi) \geq \mathcal{L}(\mathbf{s}_m^*|\mathbf{s}_n, \Psi)) \quad (3)$$

where  $\mathbf{s}_m^*$  is a random vector representing the scores calculated between pairs of objects involving at least one trace object truly originating from the same source as the control objects. The distribution of  $\mathbf{s}_m^*|\mathbf{s}_n, \Psi$  is obtained by using the structure of the covariance matrix defined in (2), such that

$$\mathbf{s}_m^*|\mathbf{s}_n, \Psi \sim MVN(\theta\mathbf{1}_m + \Sigma_{m \times m}\Sigma_{m \times n}^{-1}(\mathbf{s}_n - \theta\mathbf{1}_n), \Sigma_{m \times m} - \Sigma_{m \times n}\Sigma_{n \times n}^{-1}\Sigma_{n \times m}), \quad (4)$$

Using this test statistic, we then decide to reject  $H_1$  at a specific  $\alpha$ -level if

$$T(\mathbf{s}_m, \mathbf{s}_n, \Psi) \leq c(\alpha) \quad (5)$$

where  $c(\alpha)$  is a constant chosen to satisfy

$$\Pr(T(\mathbf{s}_m, \mathbf{s}_n, \Psi) \leq c(\alpha)) \leq \alpha \quad (6)$$

For a well-behaved test,  $c(\alpha) = \alpha$ . In practice, there is uncertainty about  $\Psi$  and the distribution of  $T(\mathbf{s}_m, \mathbf{s}_n, \Psi)$  under  $H_1$  is unknown. Thus,  $c(\alpha)$  enables us to formally control the Type I error rate of our test.

The chosen test statistic has some interesting properties:

1.  $\mathcal{L}(\mathbf{s}_m|\mathbf{s}_n, \Psi)$  decreases as the level of dissimilarity between the trace and control objects increases; hence,  $T(\mathbf{s}_m, \mathbf{s}_n, \Psi)$  will tend to 0 as the dissimilarity between trace and control objects increases. Therefore,  $T(\mathbf{s}_m, \mathbf{s}_n, \Psi)$  is a strictly positive function and the test defined in (5) is a left tail test;

2.  $\mathcal{L}(\mathbf{s}_m|\mathbf{s}_n, \Psi)$  only requires  $\mathbf{s}_m$  to be random and considers  $\mathbf{s}_n$  fixed. This enables the test statistic to be “anchored” on the characteristics observed on the control objects sampled from the specific source considered under  $H_1$ . This is especially important when the trace objects are not from the source of the control objects.

### 3.2 Accounting for the uncertainty on $\Psi$ under $H_1$

In most situations,  $\Psi$  is not known and must be learned from  $\mathbf{s}_n$ . Armstrong et al. (2017) show that an analytical solution to estimate  $\Psi$  from  $\mathbf{s}_n$  exists. Instead of replacing  $\Psi$  by a point estimate,  $\hat{\Psi}$ , in (3), we integrate out the uncertainty associated with the model parameters by considering the posterior distributions of  $\theta$ ,  $\sigma_a^2$ , and  $\sigma_e^2$  given  $\mathbf{s}_n$ . In this context, we decide to reject  $H_1$  if

$$\int T(\mathbf{s}_m, \mathbf{s}_n, \Psi) d\pi(\Psi|\mathbf{s}_n) \leq c(\alpha). \quad (7)$$

The posterior distribution  $\pi(\Psi|\mathbf{s}_n)$  is not a standard normal-inverse gamma distribution due to the coupling of  $\sigma_a^2$  and  $\sigma_e^2$  in the covariance matrix of the likelihood function of  $\mathbf{s}_n$ ,  $\Sigma_{n \times n} = \mathbf{P}\mathbf{P}^t \sigma_a^2 + \mathbf{I}_n \sigma_e^2$ . It is trivial enough to develop a Gibbs sampler to obtain a sample from the distribution. Nevertheless, as we will see in Section 4.1, it is not necessary. The integral in (7) can easily be estimated by simulation using Algorithm 1.

---

**Algorithm 1:** Simulation to estimate  $\int T(\mathbf{s}_m, \mathbf{s}_n, \Psi) d\pi(\Psi|\mathbf{s}_n)$

---

**Data:** A vector of  $N + M$  scores

**Result:**  $\int T(\mathbf{s}_m, \mathbf{s}_n, \Psi) d\pi(\Psi|\mathbf{s}_n)$

**for**  $k \in 1 : K$  **do**

1. Sample  $\Psi^{(k)} := \left\{ \sigma_a^{2(k)}, \sigma_e^{2(k)}, \theta^{(k)} \right\}$  from  $\pi(\sigma_a^2|\mathbf{s}_n)$ ,  $\pi(\sigma_e^2|\mathbf{s}_n)$ , and  $\pi(\theta|\mathbf{s}_n, \sigma_a^2, \sigma_e^2)$ ;
2. Compute the likelihood of the observed scores,  $\mathbf{s}_m$ , given  $\Psi^{(k)}$ ,  $\mathcal{L}(\mathbf{s}_m|\mathbf{s}_n, \Psi^{(k)})$ ;
3. Sample a new vector of scores,  $\mathbf{s}_m^{*(k)}$ , from  $\mathbf{s}_m^*|\mathbf{s}_n, \Psi^{(k)}$ ;
4. Compute the conditional likelihood  $\mathcal{L}(\mathbf{s}_m^{*(k)}|\mathbf{s}_n, \Psi^{(k)})$ ;
5. Determine  $L(\mathbf{s}_m^{*(k)}, \mathbf{s}_m, \mathbf{s}_n, \Psi^{(k)}) = \mathbb{I} \left( \mathcal{L}(\mathbf{s}_m|\mathbf{s}_n, \Psi^{(k)}) \geq \mathcal{L}_k(\mathbf{s}_m^{*(k)}|\mathbf{s}_n, \Psi^{(k)}) \right)$ ,  
where  $\mathbb{I}(\cdot)$  is the indicator function;

**end**

Use  $\frac{1}{K} \sum_{k=1}^K L(\mathbf{s}_m^{*(k)}, \mathbf{s}_m, \mathbf{s}_n, \Psi^{(k)})$  to estimate the integral in equation (7).

---



The output of Algorithm 1 converges to  $\int T(\mathbf{s}_m, \mathbf{s}_n, \Psi) d\pi(\Psi|\mathbf{s}_n)$  as  $k \rightarrow \infty$ , since

$$\begin{aligned}
\int T(\mathbf{s}_m, \mathbf{s}_n, \Psi) d\pi(\Psi|\mathbf{s}_n) &= \int \Pr(\mathcal{L}(\mathbf{s}_m^*|\mathbf{s}_n, \Psi) \leq \mathcal{L}(\mathbf{s}_m|\mathbf{s}_n, \Psi)) d\pi(\Psi|\mathbf{s}_n) \\
&= \int \left[ \int \mathbf{I}(\mathcal{L}(\mathbf{s}_m^*|\mathbf{s}_n, \Psi) \leq \mathcal{L}(\mathbf{s}_m|\mathbf{s}_n, \Psi)) d\pi(\mathbf{s}_m^*|\mathbf{s}_n, \Psi) \right] d\pi(\Psi|\mathbf{s}_n) \\
&= \int \mathbf{I}(\mathcal{L}(\mathbf{s}_m^*|\mathbf{s}_n, \Psi) \leq \mathcal{L}(\mathbf{s}_m|\mathbf{s}_n, \Psi)) d\pi(\mathbf{s}_m^*, \Psi|\mathbf{s}_n) \\
&= \lim_{k \rightarrow \infty} \frac{1}{K} \sum_{k=1}^K \mathbf{I}(\mathcal{L}(\mathbf{s}_{m_k}^*|\mathbf{s}_n, \Psi) \leq \mathcal{L}(\mathbf{s}_m|\mathbf{s}_n, \Psi))
\end{aligned} \tag{8}$$

### 3.3 Determining $c(\alpha)$

In most situations, the distribution of  $T(\mathbf{s}_m, \mathbf{s}_n, \Psi)$  may not be uniform since  $\Psi$  is unknown. Therefore, we must determine  $c(\alpha)$  empirically. This can be achieved in several ways depending on whether we want to condition  $c(\alpha)$  on  $\mathbf{s}_n$ , or have a decision point that will ensure an average Type I error rate across all possible sources in a population. Algorithms 2 and 3 allow for determining  $c(\alpha)$  in these two situations.

---

**Algorithm 2:** Simulation to determine  $c(\alpha)$  conditioned on  $\mathbf{s}_n$

---

**Data:** A vector of pairwise scores,  $\mathbf{s}_n$ , between  $N$  control objects.

**Result:**  $c(\alpha)$  conditioned on  $\mathbf{s}_n$

Obtain some estimate of  $\Psi$  using  $\mathbf{s}_n$ , such as  $\tilde{\Psi}$ , the mode of  $\pi(\theta, \sigma_a^2, \sigma_e^2|\mathbf{s}_n)$ ;

**for**  $j \in 1 : J$  **do**

- 1. Generate  $\tilde{\mathbf{s}}_{m_j} \sim \mathbf{s}_m|\mathbf{s}_n, \tilde{\Psi}$  using equation (4);
- 2. Use Algorithm 1 to approximate  $p_j = \int T(\tilde{\mathbf{s}}_{m_j}, \mathbf{s}_n, \Psi) d\pi(\Psi|\mathbf{s}_n)$ ;

**end**

Define  $c(\alpha)$  as the  $\alpha$ -percentile of the empirical distribution of the  $p_j$ .

---

Conditioning  $c(\alpha)$  on  $\mathbf{s}_n$  implies that the test is specific to the observed control objects. This presents the advantage of only needing the  $N$  observations made on the control objects:  $c(\alpha)$  can be entirely determined by simulations. However, in this situation,  $c(\alpha)$  relies heavily on the assumption of normality of the distribution of the scores to obtain the  $\tilde{\mathbf{s}}_m$ 's. Furthermore, Figures 1 and 2(left) show that this strategy does not guarantee

that the true Type I error rate for the source considered under  $H_1$  will be  $\alpha$ . Indeed, the observed vector of scores  $\mathbf{s}_n$  may be far from its expectation. In such case, our test may lack power and erroneously include traces from sources that are more likely to have generated the control objects than the true source. Additionally, the test may be overly discriminating and exclude trace samples from the true source at a higher rate than  $\alpha$  (as in Figure 2(left)). Hence, conditioning  $c(\alpha)$  on  $\mathbf{s}_n$  may results in a poorly performing test when the  $N$  control objects are not typical of their source. This phenomenon can also be observed by simulation using a simple  $z$ -test.

---

**Algorithm 3:** Simulation to determine  $c(\alpha)$  across all sources

---

**Data:** A database of  $I$  distinct sources

**Result:** Unconditioned  $c(\alpha)$  for all sources

**for**  $i \in 1 : I$  sources **do**

**for**  $j \in 1 : J$  **do**

1. Sample  $N_{ij}$  control objects from source  $i$  in the database;
2. Generate  $M_{ij}$  trace objects that correspond to source  $i$  in the database;
3. Compute all pairwise scores,  $\tilde{\mathbf{s}}_{ij} = \begin{pmatrix} \tilde{\mathbf{s}}_{m_{ij}} \\ \tilde{\mathbf{s}}_{n_{ij}} \end{pmatrix}$ ;
4. Use Algorithm 1 to approximate  $p_{ij} = \int T(\tilde{\mathbf{s}}_{m_{ij}}, \tilde{\mathbf{s}}_{n_{ij}}, \Psi) d\pi(\Psi | \tilde{\mathbf{s}}_{n_{ij}})$ ;

**end**

**end**

Define  $c(\alpha)$  as the  $\alpha$ -percentile of the empirical distribution of the  $p_{ij}$ .

---

The unconditional  $c(\alpha)$ , obtained using Algorithm 3, has two main advantages: it can be determined for a type of evidence based on a large validation experiment prior to the introduction of the method in casework; furthermore, by construction, it will guarantee that the overall Type I error for the considered type of evidence will be at least  $\alpha$  (Figure 2(right)), even though it might be higher or lower for a particular source. However, determining  $c(\alpha)$  using this strategy requires a large number of samples from a large number of sources, and makes the test less specific to the case at hand.

### 3.4 Power of the test

The power of the test introduced in Sections 3.1 and 3.2 can be determined empirically by using a reference library of sources that are known to have different characteristics in the input space (e.g., the same collection of sources that was used to determine  $c(\alpha)$  in Algorithm 3). Using these objects, it is possible to empirically determine the power of the test for the specific source considered by  $H_1$ , and for fixed numbers of trace and control objects, by

1. Selecting  $N$  objects from the source considered by  $H_1$
2. Considering the library of sources as sources for trace objects, and selecting each reference source in turn;
3. Estimating the integral in (7) using  $M$  objects from the selected reference source and keeping the  $N$  control objects fixed;
4. Expressing the integral in (7) as a function of the average level of dissimilarity between the trace objects from the selected source from the library and the control objects.

We stress that the power of our test for a specific  $\alpha$ -level is not equivalent to the match probability assigned during the second of the two stages of our approach. The power of the test is determined using sources that are known to have characteristics that are different from each other, while the second stage of the approach requires to consider a simple random sample of sources from a population.

## 4 Computational considerations

Calculating  $\frac{1}{K} \sum_{k=1}^K L(\mathbf{s}_m^{*(k)}, \mathbf{s}_m, \mathbf{s}_n, \Psi^{(k)})$  in Algorithm 1 requires posterior samples from  $\Psi|\mathbf{s}_n$ , and  $\mathbf{s}_m|\mathbf{s}_n, \Psi^{(k)}$  at each iteration of the algorithm. We face three challenges when calculating  $\frac{1}{K} \sum_{k=1}^K L(\mathbf{s}_m^{*(k)}, \mathbf{s}_m, \mathbf{s}_n, \Psi^{(k)})$  for large  $K$  or  $N$ :

1. Using a Gibbs sampler to obtain a sample from  $\pi(\Psi|\mathbf{s}_n)$  involves a great many number of iterations to obtain a reasonable sample size for  $\Psi$  due to the need to account for the burn-in period and thinning.

2. Sampling from  $\pi(\theta|\sigma_a^2, \sigma_e^2, \mathbf{s}_n)$  requires calculating the determinant and inverse of  $\Sigma_{n \times n}$  for each new value of  $\sigma_a^2$  and  $\sigma_e^2$ ; this may quickly become cumbersome depending on the dimension of  $\mathbf{s}_n$  and the number of samples needed;
3. Similarly, sampling from  $\pi(\mathbf{s}_m|\mathbf{s}_n, \Psi^{(k)})$  requires calculating the determinant and inverse of the conditional covariance matrix  $\Sigma_{m \times m} - \Sigma_{m \times n} \Sigma_{n \times n}^{-1} \Sigma_{n \times m}$  in (4) for each new sample  $\Psi^{(k)}$ ; again, this may become a challenge as the dimensions of  $\mathbf{s}_n$  and  $\mathbf{s}_m$ , and the number of samples needed increase.

In the following sections, we propose solutions that allow for removing these computational bottlenecks, and enable us to use Algorithm 1 with large values for  $K$ ,  $M$  and  $N$ .

#### 4.1 Posterior sample from $\pi(\Psi|\mathbf{s}_n)$

Rather than using a Gibbs sampler to obtain posterior samples from  $\pi(\Psi|\mathbf{s}_n)$ , we capitalise on the fact that the sums of squares,  $SS_a$  and  $SS_e$ , used in the estimation of  $\sigma_a^2$  and  $\sigma_e^2$  in (Armstrong et al., 2017), are independent, such that

$$\begin{aligned} \frac{SS_a}{(n-2)\sigma_a^2 + \sigma_e^2} &\sim \chi_{df=N-1}^2 \\ \frac{SS_e}{\sigma_e^2} &\sim \chi_{df=n-N}^2. \end{aligned} \tag{9}$$

Defining  $\eta_a$  and  $\eta_e$  as the natural parameters of  $SS_a$  and  $SS_e$ , we can sample from

$$\begin{aligned} \pi(\eta_a|SS_a) &\propto f(SS_a|\eta_a)\pi(\eta_a) \\ \pi(\eta_e|SS_e) &\propto f(SS_e|\eta_e)\pi(\eta_e). \end{aligned} \tag{10}$$

Assuming inverse-gamma conjugate prior distributions for  $\eta_a$  and  $\eta_e$ , we have that

$$\begin{aligned} \pi(\eta_a|SS_a, \alpha_a, \beta_a) &\sim IG\left(\alpha_a + \frac{N-1}{2}, \frac{SS_a}{2} + \beta_a\right) \\ \pi(\eta_e|SS_e, \alpha_e, \beta_e) &\sim IG\left(\alpha_e + \frac{n-N}{2}, \frac{SS_e}{2} + \beta_e\right). \end{aligned} \tag{11}$$

Finally, using the ANOVA table in Armstrong et al. (2017), we can obtain a joint sample of  $\sigma_a^2$  and  $\sigma_e^2$  from a sample of  $\eta_a$  and  $\eta_e$  using

$$\begin{bmatrix} \sigma_a^2 \\ \sigma_e^2 \end{bmatrix} = \begin{bmatrix} N-1 & 1 \\ 0 & 1 \end{bmatrix}^{-1} \begin{bmatrix} \eta_a \\ \eta_e \end{bmatrix} \tag{12}$$

Similarly, we can obtain a posterior sample for  $\theta$  from a joint sample of  $\sigma_a^2$  and  $\sigma_e^2$  by assuming a normal prior

$$\begin{aligned}\pi(\theta|\mathbf{s}_n, \sigma_a^2, \sigma_e^2) &\propto \mathcal{L}(\mathbf{s}_n|\sigma_a^2, \sigma_e^2, \theta)\pi(\theta|\theta_0, \lambda) \\ &= MVN(\mathbf{1}_n\theta, \Sigma_{n \times n})N(\theta_0, \lambda) \\ &= N(\mu_p, \sigma_p^2),\end{aligned}\tag{13}$$

where

$$\begin{aligned}\mu_p &= \frac{\mathbf{s}_n^t \Sigma_{n \times n}^{-1} \mathbf{1}_n + (\lambda(2\sigma_a^2 + \sigma_e^2))^{-1} \theta_0}{\mathbf{1}_n^t \Sigma_{n \times n}^{-1} \mathbf{1}_n + (\lambda(2\sigma_a^2 + \sigma_e^2))^{-1}} \\ \sigma_p^2 &= \mathbf{1}_n^t \Sigma_{n \times n}^{-1} \mathbf{1}_n + (\lambda(2\sigma_a^2 + \sigma_e^2))^{-1}.\end{aligned}\tag{14}$$

Note that we are not concerned with the choice of the hyperparameters: different choices of prior for  $\Psi$  may be considered (e.g., subjective, uninformative, or obtained from the empirical study of a large sample from a population of objects).

This approach allows us to directly generate iid samples from  $\pi(\Psi|\mathbf{s}_n)$ . It does not require a burn-in period, or thinning, and therefore, does not waste computational resources. However, this approach still requires calculating the determinant and inverse of  $\Sigma_{n \times n}$  for each sample of  $\sigma_a^2$  and  $\sigma_e^2$  to obtain a new sample of  $\theta$ .

## 4.2 Determinant and inverse of $\Sigma_{n \times n}$

We avoid the computational cost of repeatedly inverting  $\Sigma_{n \times n}$  by taking advantage of its spectral decomposition. Armstrong et al. (2017) show that  $\Sigma_{n \times n}$  has three different eigenvalues

$$\lambda_1 = 2(N-1)\sigma_a^2 + \sigma_e, \quad \lambda_2 = (N-2)\sigma_a^2 + \sigma_e^2, \quad \lambda_3 = \sigma_e^2\tag{15}$$

with multiplicity 1,  $N-1$ , and  $n-N$  respectively. They also show that

$$\Sigma_{n \times n}^{-1} = \frac{\mathbf{v}_1 \mathbf{v}_1^t}{\lambda_1} + \sum_{k=2}^n \frac{\mathbf{v}_k \mathbf{v}_k^t}{\lambda_2} + \sum_{k=n+1}^N \frac{\mathbf{v}_k \mathbf{v}_k^t}{\lambda_3}\tag{16}$$

where  $\mathbf{v}_1 = \frac{\mathbf{1}_n}{\sqrt{n}}$  and  $\mathbf{v}_k$  are eigenvectors orthogonal to  $\mathbf{v}_1$ , and calculate that

$$\begin{aligned}\sum_{k=2}^n \mathbf{v}_k \mathbf{v}_k^t &= \frac{(N-1)^2}{N-2} \left( \frac{1}{N-1} \mathbf{P} - \frac{1}{n} \mathbf{1}_n \mathbf{1}_n^t \right) \left( \frac{1}{N-1} \mathbf{P}^t - \frac{1}{n} \mathbf{1}_n \mathbf{1}_n^t \right) \\ \sum_{k=N+1}^n \mathbf{v}_k \mathbf{v}_k^t &= \mathbf{I}_n - \mathbf{v}_1 \mathbf{v}_1^t - \sum_{k=2}^N \mathbf{v}_k \mathbf{v}_k^t\end{aligned}\tag{17}$$

Since  $N$  is fixed, the general structure of  $\Sigma_{n \times n}$  is fixed. Thus, to obtain  $\Sigma_{n \times n}$  for any new values of  $\sigma_a^2$  and  $\sigma_e^2$ , only the eigenvalues have to be recalculated. This enables us to efficiently obtain the new value for the determinant of  $\Sigma_{n \times n}$  and the inverse of that matrix at each iteration of Algorithm 1.

### 4.3 Resampling from $\mathbf{s}_m | \mathbf{s}_n, \Psi^{(k)}$

To generate samples of scores from  $\mathbf{s}_m | \mathbf{s}_n, \Psi^{(k)} \sim MVN(\boldsymbol{\mu}_{\mathbf{s}_m | \mathbf{s}_n, \Psi^{(k)}}, \Sigma_{\mathbf{s}_m | \mathbf{s}_n, \Psi^{(k)}})$  in (4), we exploit the properties of the Cholesky decomposition of  $\Sigma_{\mathbf{s}_m | \mathbf{s}_n, \Psi^{(k)}} = \Sigma_{m \times m} - \Sigma_{m \times n} \Sigma_{n \times n}^{-1} \Sigma_{n \times m}$ . We define  $\Sigma_{\mathbf{s}_m | \mathbf{s}_n, \Psi^{(k)}} := \mathbf{L}\mathbf{L}^t$ , where  $\mathbf{L}$  is a lower triangular matrix. It follows that any vector  $\mathbf{s}_m^{*(k)} = \boldsymbol{\mu}_{\mathbf{s}_m | \mathbf{s}_n, \Psi^{(k)}} + \mathbf{L}\mathbf{z}$ , where  $\mathbf{z} \in \mathbb{R}^m$  and  $z_i \sim N(0, 1)$ , has mean  $\boldsymbol{\mu}_{\mathbf{s}_m | \mathbf{s}_n, \Psi^{(k)}}$  and covariance  $\Sigma_{\mathbf{s}_m | \mathbf{s}_n, \Psi^{(k)}}$ , and thus is a sample from  $\pi(\mathbf{s}_m | \mathbf{s}_n, \Psi^{(k)})$ . While  $\mathbf{L}$  has to be recalculated for each new sample of  $\Psi^{(k)}$ , calculating the Cholesky decomposition of  $\Sigma_{\mathbf{s}_m | \mathbf{s}_n, \Psi^{(k)}}$  is significantly faster than determining its inverse by other methods.

## 5 Second stage: assigning the *probability of match*

The focus of the second stage of the approach is to assess the contribution of the decision that the sources of the trace and control objects are indistinguishable to the inference process (the second stage is not performed when the first stage results the rejection of the hypothesis of common source at the selected  $\alpha$ -level). This value is a function of the number of sources, in a population of potential sources, that are also indistinguishable from the source of the trace objects. Thus, the second stage aims at assigning a so-called “probability of match”. Ideally, assigning this probability would require some knowledge of the way the characteristics observed on the trace are distributed over the population of potential sources; in turn, this would require defining a likelihood function, which, we mentioned previously, may not exist for most forensic evidence types.

Instead, for the time being, we propose to follow Parker (1967), and repeatedly test each source from a sample of sources from the population of potential sources using Algorithm 1, keeping  $c(\alpha)$  fixed. This process allows to use the relative frequency of indistinguishable sources as a proxy for the match probability. This process consists in performing multiple

dependent  $\alpha$ -level tests, since the  $M$  trace objects are common to all tests. The quality of the relative frequency of indistinguishable sources as an estimate of the match probability depends on how the Type I and Type II errors combine across these different tests. We are currently working on methods to propose a solution to the issue of multiple dependent testing in the context of the proposed model.

## 6 Worked example

In this section, we present a worked example of the proposed approach using Fourier-transform infrared spectroscopy (FTIR) analysis of paint chips. Our example is based on seven FTIR spectra acquired from seven different paint samples from one can of household paint. Each spectra represents the absorbance of the paint material for a range of wavelengths (from 550 to 4,000  $\text{cm}^{-1}$ ). We use a lag 2 cross-correlation function to compare our spectra.

For the purpose of this example, we treat the spectra as functional data and express each one as a linear combination of 100 B-spline bases. We assume that the vectors of basis coefficients are iid multivariate normal and use the sample mean and covariance matrix of the coefficients for the seven spectra as point estimates for the parameters of their distribution. This is obviously not a very good estimate, but it is fit-for-purpose in the context of this example, and this strategy enables us to “resample new spectra” from the considered source in order to study the behaviour of our model under different conditions. This strategy also allows us to obtain spectra from “different sources” by (i) performing an eigen-decomposition on the sample covariance matrix of the basis coefficients of the seven observed spectra, (ii) obtaining the coordinates of the mean vector of the basis coefficients in the space defined by the eigenfunctions obtained in (i), (iii) varying the element of that vector corresponding to one of the eigenfunctions and (iv) reconstructing the vector of basis coefficients in the original input space. The reconstructed vectors of basis coefficients can then be used as mean vectors for the multivariate normal distribution used to simulate spectrum objects that increasingly differ from the observed spectra. Figure 1 presents the seven observed spectra (bottom), and simulated spectra from the same can of household paint (top).

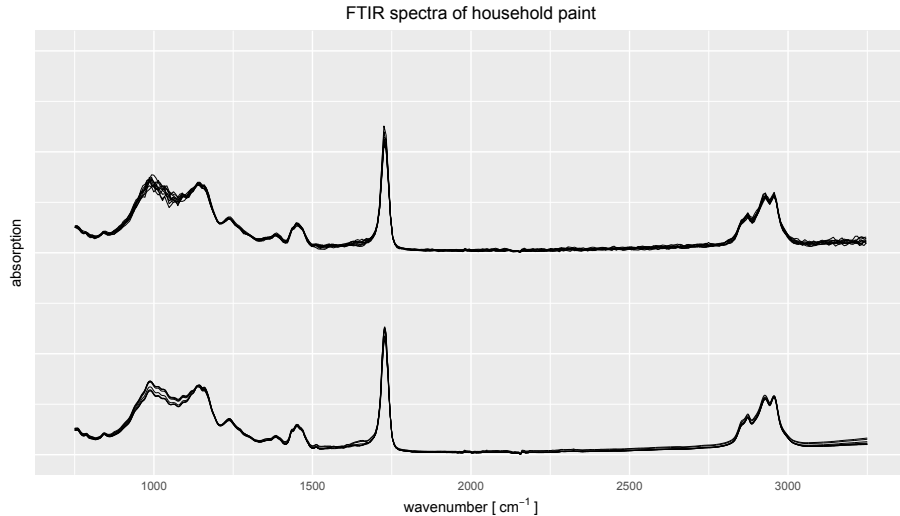


Figure 1: Bottom: observed FTIR spectra. Top: simulated FTIR spectra under  $H_1$

Figure 2 shows distributions of the test statistic,  $\int T(\mathbf{s}_m, \mathbf{s}_n, \Psi) d\pi(\Psi | \mathbf{s}_n)$ , under  $H_1$  and  $H_2$  for the conditional and unconditional situations considered in Section 3.3. In Figure 2(left), each value of the test statistic is obtained using the same  $N = 10$  simulated control spectra that are kept fixed during the entire experiments. The dashed line in Figure 2(left) represents the distribution of the test statistic obtained using Algorithm 2 by resampling  $\tilde{\mathbf{s}}_m$  for  $M = 2$ . The solid curves represent the distribution of the test statistics obtained using Algorithm 1 with  $M = 2$  simulated trace spectra from the true source (solid black line) and  $M = 2$  simulated spectra from sources under  $H_2$  (solid grey curves).

We can see that the distribution of the test statistic in the dashed line diverges slightly from  $Unif(0, 1)$ . We can use this distribution function to empirically control the  $\alpha$ -level of the test (Table 1) by obtaining the corresponding conditional  $c(\alpha) | \mathbf{s}_n$ , instead of simply assuming that  $c(\alpha) = \alpha$ . For the particular choice of  $\mathbf{s}_n$  presented in Figure 2(left), the distribution function represented by the dashed line is clearly different from the distribution function of  $\int T(\mathbf{s}_m, \mathbf{s}_n, \Psi) d\pi(\Psi | \mathbf{s}_n)$  obtained by directly simulating  $M$  trace spectra from the true source of the  $N$  control spectra. Furthermore, the dashed distribution partially dominates a distribution of the test statistic obtained under  $H_2$ .

The results presented in Figure 2(left) have at least two implications. First, the  $\alpha$ -level of the test is specific to the observed  $\mathbf{s}_n$  and does not reflect the true rate of erroneous rejection of  $H_1$  for the true source of the  $N$  control objects. This situation arises when  $\mathbf{s}_n$  is not



Table 1:  $\alpha$  and corresponding  $c(\alpha)$  associated with ecdf of (top row) conditional  $p_j$  from Algorithm 2 and (bottom row) unconditional  $p_{ij}$  from Algorithm 3. The bolded column gives the value of  $c(\alpha)$  for  $\alpha = 0.15$ , corresponding to the vertical lines in Figure 2.

$\alpha$ - level	0.05	<b>0.15</b>	0.25	0.50	0.75	0.95	0.99
$c(\alpha) \mathbf{s}_n$	0.0598	<b>0.145</b>	0.2185	0.4155	0.668	0.89205	0.9552
$c(\alpha)$	0.0000	<b>0.0117</b>	0.07575	0.44	0.79525	0.99205	1.0000

typical of the scores that could be observed between objects of the considered source. The  $\alpha$ -level of the test for the true source may be higher or lower than the  $\alpha$ -level corresponding to the choice of  $c(\alpha)$ . Second, our results show that a decision of distinguishability based on  $c(\alpha)$  would lack power and potentially erroneously include many sources under  $H_2$  when these sources only slightly differ from the source considered under  $H_1$ . Figure 3(bottom) shows an excerpt of the different simulated sources considered in Figure 2(left) with matching colour codes. We can see in Figure 3(bottom) that the pattern of the spectra with the darker shade of grey appear more similar to the one of the spectra represented by the black solid line, which is consistent with the data presented in Figure 2(left). Overall, conditioning the choice of  $c(\alpha)$  on the observed  $\mathbf{s}_n$  might result in a test that is overly inclusive and detrimental to suspects that are genuinely not involved in the investigated crime.

In Figure 2(right), each value of  $\int T(\mathbf{s}_m, \mathbf{s}_n, \Psi)d\pi(\Psi|\mathbf{s}_n)$  is obtained by resampling trace and control objects for each iteration of Algorithm 3. Each of the curves represents the distribution of the test statistic obtained using Algorithm 1, with  $N = 10$  simulated control spectra and  $M = 2$  simulated trace spectra. The solid black line represents trace spectra simulated under  $H_1$ , while the grey curves represent trace spectra from sources simulated under  $H_2$ . We can see that the distribution of the test statistic given by the solid black line diverges from  $Unif(0, 1)$  by a great deal. As before, we can use this distribution function to empirically control the  $\alpha$ -level of the test (Table 1) by obtaining the corresponding unconditional  $c(\alpha)$ , instead of assuming that  $c(\alpha) = \alpha$ .

We can see that the distribution function given by the solid black line does not dominate any of the other distributions of  $\int T(\mathbf{s}_m, \mathbf{s}_n, \Psi)d\pi(\Psi|\mathbf{s}_n)$  obtained under  $H_2$ . We can

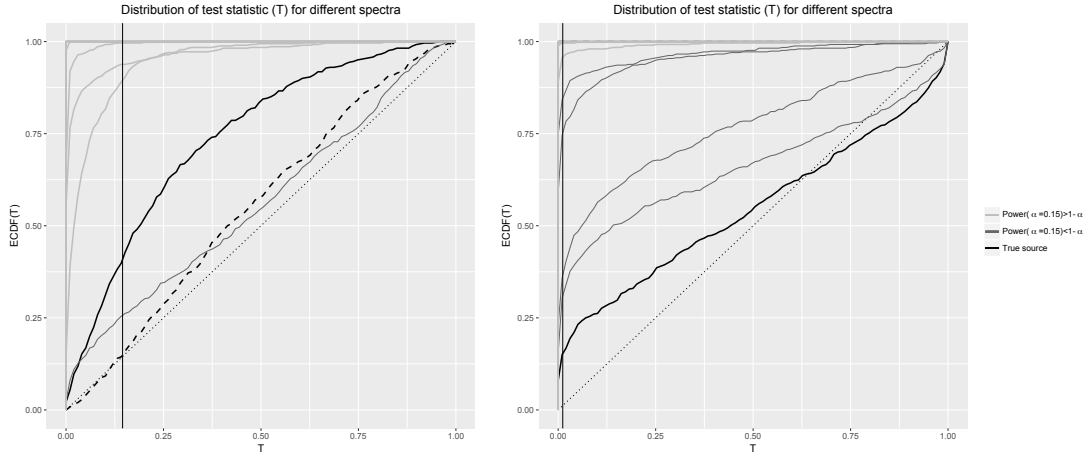


Figure 2: Empirical cumulative distribution functions (ECDFs) of  $\int T(\mathbf{s}_m, \mathbf{s}_n, \Psi) d\pi(\Psi | \mathbf{s}_n)$  under different scenarios with  $N = 10$  and  $M = 2$ . The vertical line represents  $c(\alpha)$  corresponding to  $\alpha = 0.15$ . The solid black ECDFs corresponds to the test statistics obtained by resampling trace spectra from the source considered under  $H_1$ . ECDFs from the test statistics obtained using trace samples from the sources considered under  $H_2$  are in grey. Lighter grey indicates that the trace samples associated with these spectra have more power to detect differences from the control samples. Left:  $c(\alpha)$  is determined using Algorithm 2. The black dashed ECDF corresponds to the test statistics calculated using Algorithm 2 for the observed  $\mathbf{s}_n$ . Right:  $c(\alpha)$  is determined using Algorithm 3.

conclude that there are no other sources that will be accepted at a higher rate than the true source since their power is higher than  $\alpha$ . The explanation of this observation lies in that, by constantly resampling both trace and control objects from a common source, we obtain a good representation of the average distribution of the test statistic under  $H_1$ . We also note that the value of unconditional  $c(\alpha)$  (Table 1) is very small for the selected  $\alpha$ . This implies that many more observations are required to ensure the precision of  $c(\alpha)$  and to guarantee that the type I error and the power of the test are stable. Indeed, for very small values of  $c(\alpha)$ , any variations of  $c(\alpha)$  due to sampling effects in Algorithm 3 may result in drastic changes in the power of the test. Finally, we note that Figure 2(right) is not a true representation of the distribution of  $\int T(\mathbf{s}_m, \mathbf{s}_n, \Psi) d\pi(\Psi|\mathbf{s}_n)$  that should be obtained through Algorithm 3. In practice, sampling from a single source to obtain the distribution of  $\int T(\mathbf{s}_m, \mathbf{s}_n, \Psi) d\pi(\Psi|\mathbf{s}_n)$  under  $H_1$  would require an unrealistic number of samples from that source. Furthermore, this would require to determine  $c(\alpha)$  each time a new source is considered. We chose to focus on a single source in the context of this example to illustrate the behaviour of our model in the two situations. We are currently collecting the necessary data to validate the performance of our proposed approach in an operational environment.

Lastly, by considering Figure 3, we can see that using an unconditional  $c(\alpha)$  has the potential to make the test less discriminative. This is reflected by the greater number of sources (solid dark grey curves) that would be considered indistinguishable from the true source when using the threshold determined by the unconditional  $c(\alpha)$  (Figure 3(top)) versus when using the threshold determined by the conditional  $c(\alpha)$  (Figure 3(bottom)). Upon collecting the necessary data, we will be able to explore this behaviour in greater detail.

## 7 Benefits and limitations of the two-stage approach

While the two-stage approach was proposed several decades ago, very little work has been done to formalise and develop it. Nevertheless, this approach has several advantages over the more commonly advocated Bayes factor, and it is not surprising that the value of many evidence types is assessed using some form of (possibly informal) two-stage approach.

Firstly, the flow of the two-stage approach appears natural to forensic scientists, legal

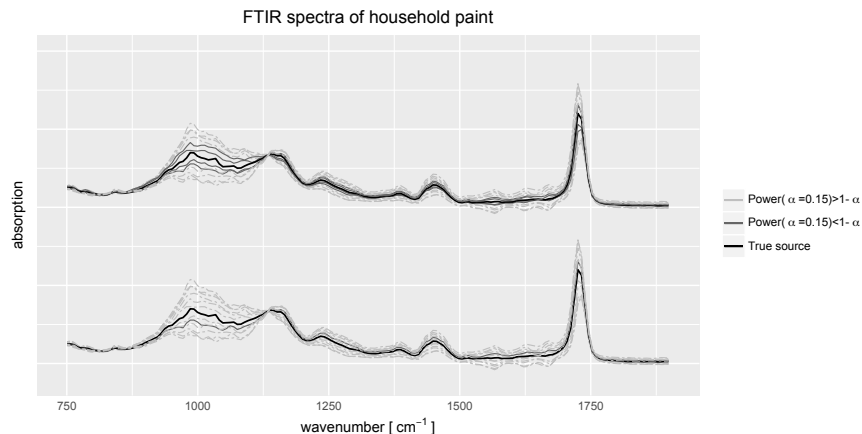


Figure 3: Magnification of the first series of peaks of simulated FTIR spectra under  $H_1$  and  $H_2$ . Bottom: Spectra classified according to threshold determined by conditional  $c(\alpha)$ . Top: Spectra classified according to threshold determined by unconditional  $c(\alpha)$ . The spectra from the source considered under  $H_1$  are represented in black; spectra from the sources considered under  $H_2$  are in grey. Lighter grey indicates that the trace samples associated with these spectra have more power to detect differences from the control samples.

practitioners and lay individuals: (1) the trace and control objects are compared to determine if they could come from the same source; (2) if the two sets of objects are considered *similar*, the implications of this finding is assessed. Each stage focuses on its own specific question. Because the two stages appear so well separated, yet logically connected, they are easy to explain, and even easier to understand by a lay audience, such as a jury (Neumann et al., 2016). Scientists can discuss their conclusions for each stage in turn, and how they fit into the overall inference problem. In addition, the issue of error rates naturally occurs in relation to the decision that has to be made at the end of the first stage. The clarity of the two-stage approach to lay individuals has to be put in perspective with the confusion that usually occurs, even among scientists and legal practitioners, when they are asked to use a Bayes factor to update their prior beliefs on the source of trace samples.

Secondly, performing Bayesian model selection using high-dimension complex data requires using intractable likelihood functions or even probability measures that may not exist in the input space of the data. In addition, data dimension reduction techniques, such as principal component analysis, may engender loss of information that may impact

the weight of the evidence in unpredictable ways (e.g., the wrong model may end up being supported at an unknown rate) and may not be applicable to heterogeneous complex data types. On the contrary, it is almost always possible to design a test statistic, study its distribution empirically using a large sample of pairs of objects from the same source, and control the  $\alpha$ -level of the test, even in the context of high-dimensional complex data.

In this paper, we propose a semi-parametric model that offers several major advantages over a fully empirical approach:

1. Assuming that our decision criteria is an unconditional  $c(\alpha)$ , for the reasons discussed in the previous section, and that the value of  $c(\alpha)$  for the desired  $\alpha$ -level has been obtained, using the test only requires considering the observations made on the trace and control objects;
2. The test accounts for the specific characteristics of the source of the control objects;
3. The same test statistic can be used for any type or dimension of data. It can be tailored to the data through the use of a kernel function. In addition, the kernel function can be designed to maximise the power of the test by maximising the distance between objects originating from different sources and minimising the distances between objects originating from a common source. Finally, by using the different properties of kernels, the function can be designed to ensure that the main assumption of the model, the normality of the score distribution under  $H_1$ , is satisfied (Schoelkopf and Smola, 2001);
4. By construction, the test statistic requires only three parameters to be considered, irrespective of the type and dimension of the raw data. We have shown in the previous sections that this enables us to implement efficient computational strategies to calculate the test statistic and study its distribution under  $H_1$  and its power given a suitable sample of sources from a population.

This paper relies on the model proposed by Armstrong et al. (2017) and assumes that the sets of objects representing the trace and the control material include one measurement for each object. The method proposed above can be expanded to include multiple measurements for each object using the score model proposed by Armstrong (2017); however,

some of the computational improvements proposed in Section 4 cannot be used and the method may involve the spectral decomposition of large matrices.

The two-stage approach suffers from several limitations, and, when possible, Bayes factors are preferred to support the inference process. The main objection to the two-stage approach rests in that evidence evaluated using this approach cannot be combined with other pieces of evidence in a logical and coherent manner (see Robertson and Vignaux (1995) for a discussion). Another major flaw has been described by Robertson and Vignaux (1995) as the “fall-of-the-cliff” effect (similar to Lindley’s paradox (Lindley, 1957)): the decision to reject the hypothesis of common source during the first stage relies only on whether the value of the test statistic is smaller or larger than a given threshold, and not on the magnitude of the distance between the test statistic and the threshold. Values of the test statistic just beyond the decision threshold will result in a drastically different decision (i.e., exclusion of the considered source) than values just before the threshold (i.e., association of the trace and control objects). In practice, this implies that the source of the control objects is either unequivocally excluded as the source of the trace objects (if  $H_1$  is rejected), or that the inference process exclusively favours  $H_1$  over  $H_2$  (since the match probability of the trace objects in a population of sources will always be lower or equal to 1). By design, the two-stage approach cannot result in a situation where  $H_2$  is favoured compared to  $H_1$  without  $H_1$  being entirely excluded. A further issue with the two-stage approach is related to the power of the test as the quality of the information contained in the trace and control objects decreases. Decreasing quantity and quality of information result in failing to reject  $H_1$  at a higher rate. For most applications of statistical hypothesis testing, this would be considered conservative. However, the situation in the forensic context is reversed: failing to reject  $H_1$  implies that the suspected source cannot be excluded, and critically, that the inference process will favour the hypothesis that the considered source is in fact the source of the trace vs. the hypothesis that the trace material originates from another source in a population of potential sources. In other words, traces with lower quality and quantity of information (i.e., bearing less discriminating features) will be easier to associate to any given suspected source. In the context of the criminal justice system, this behaviour of the test is clearly biased in favour of the prosecution.

## 8 Conclusion

In this paper, we develop and formalise a two-stage approach for the inference of the source of trace objects in a forensic context. Our approach is particularly useful when the objects are characterised by high-dimension and complex data, such as chemical spectra, for which likelihood-based inference is not possible.

Although it is not without limitations, the two-stage approach presented in this paper has several major advantages. First, our method provides a framework that enables structured and statistically rigorous inferences in forensic science. Furthermore, the two-stage approach may not be as logical and coherent as a fully Bayesian inference framework; however, because its two stages address different and well-defined issues related to the inference process, cognitive research supports that the two-stage approach is a more natural reasoning framework for forensic practitioners and lay individuals alike.

Second, the test statistic and associated likelihood structure proposed in this paper are invariant to the type and dimension of the considered data. The test statistic relies on a kernel function that can be tailored to suit any situation. Thus, the same test statistic can be used in almost any situation where high-dimension, complex and heterogenous data are considered.

Much work remains to be done before implementing this methodology in forensic practice. We are currently gathering the necessary data to calculate an unconditional decision threshold for FTIR spectra of paint samples and study the power of the test; we are developing a metric that will account for the specificity of the paint data; we are investigating the behaviour of the first stage of our approach as the ratio of trace and control objects varies; and most importantly, we are developing a model to estimate the match probability in the second stage of the approach and replace the current empirical strategy originally proposed by Parker.

## References

Aitken, C., Roberts, P., and Jackson, G. (2010). 1. fundamentals of probability and statistical evidence in criminal proceedings. In *Communicating and Interpreting Statisti-*

*cal Evidence in the Administration of Criminal Justice, Guidance for Judges, Lawyers, Forensic Scientists and Expert Witnesses.* Royal Statistical Society.

Armstrong, D. (2017). *Development and properties of kernel-based methods for the interpretation and presentation of forensic evidence.* Dissertation, South Dakota State University. <https://openprairie.sdstate.edu/etd/2175/>.

Armstrong, D., Neumann, C., Saunders, C., Gantz, D., Miller, J., and Stoney, D. (2017). Kernel-based methods for source identification using very small particles from carpet fibers. *Chemometrics and Intelligent Laboratory Systems*, 160:99–209.

Butler, J. (2015). *Advanced Topics in Forensic DNA Typing: Interpretation.* Elsevier Academic Press.

Evetts, I. (1977). The interpretation of refractive index measurements. *Forensic Science*, 9:209–217.

Kaye, D. (2017). Hypothesis testing in law and forensic science: A memorandum. *Harvard Law Review Forum*, 130(5):127–136.

Kingston, C. (1965). Applications of probability theory in criminalistics. *Journal of the American Statistical Association*, 60:70–80.

Lindley, D. (1957). A statistical paradox. *Biometrika*, 44:187–192.

Neumann, C., Kaye, D., Jackson, G., Reyna, V., and Ranadive, A. (2016). Presenting quantitative and qualitative information on forensic science evidence in the courtroom. *CHANCE*, 29:37–43.

O’Brien, A. (2017). *A Kernel Based Approach to Determine Atypicality.* Dissertation, South Dakota State University. <https://openprairie.sdstate.edu/etd/1711/>.

Parker, J. (1966). A statistical treatment of identification problems. *Journal of FSSoc*, 6:33–39.

Parker, J. (1967). The mathematical evaluation of numerical evidence. *Journal of FSSoc*, 7:134–144.



- Robertson, B. and Vignaux, G. (1995). *Interpreting Evidence: Evaluating Forensic Science in the Courtroom*. John Wiley and Sons Ltd.
- Schoelkopf, B. and Smola, A. (2001). *Learning with Kernels: Support Vector Machines, Regularization, Optimisation and Beyond (Adaptive Computation and Machine Learning)*. The MIT Press, 1 edition.
- Taroni, F., Champod, C., and Margot, P. (1999). Forerunners of bayesianism in early forensic science. *Journal of Forensic Identification*, 49:285–305.

# Appendices

## Appendix A: Summary of the main results from Armstrong et al. (2017)

Given two vectors of measurements  $\mathbf{x}_i$  and  $\mathbf{x}_j$  representing the observations made on two objects,  $i, j$ , sampled from a common source, a kernel function,  $\kappa$ , is used to measure their level of similarity and report it as a score,  $s_{i,j}$ . The score is represented by a linear random effects model

$$s_{i,j} = \kappa(\mathbf{x}_i, \mathbf{x}_j) = \theta + a_i + a_j + \epsilon_{i,j}, \quad (51)$$

where  $\theta$  is the expected value of the score between any two objects from the same considered source;  $a_i, a_j$  are random effects representing the contributions of the  $i$ th and  $j$ th objects, and  $\epsilon_{ij}$  is a lack of fit term, such that  $a_i \stackrel{iid}{\sim} N(0, \sigma_a^2)$ , and  $\epsilon_{ij} \sim N(0, \sigma_e^2)$ .

We note that the kernel function at the core of the model,  $\kappa$ , can be designed to accommodate virtually any type of data. It needs satisfy only two requirements: it must be a symmetric function, that is  $\kappa(\mathbf{x}_i, \mathbf{x}_j) = \kappa(\mathbf{x}_j, \mathbf{x}_i)$ ; and it must ensure that the marginal distribution of  $s_{ij}$  is normal to satisfy the assumption made on the score model in (51). The assumption of normality is the main assumption made by Armstrong et al. (2017) when developing their model; it is reasonable for high-dimension objects and can be satisfied through careful design of the kernel function (Armstrong, 2017).

The vector of all possible pairwise comparisons between  $N$  reference objects can be represented by a vector,  $\mathbf{s}_n$  of  $n = \binom{N}{2}$  objects, given by  $\mathbf{s}_n = (s_{1,2}, s_{1,3}, \dots, s_{n-1,n})^t$ . The multivariate extension of the model in (51) to  $\mathbf{s}_n$  is given by

$$\mathbf{s}_n = \theta \mathbf{1}_n + \mathbf{P}\mathbf{a} + \epsilon, \quad (52)$$

where  $\mathbf{1}_n$  is a one vector of length  $n$ ,  $\mathbf{P}$  is an  $n \times N$  design matrix (where each row represents a  $i, j$  combination and consists of ones in the  $i^{th}$  and  $j^{th}$  columns and zeros elsewhere),  $\mathbf{a}$  is the vector of random effects for the considered objects, and  $\epsilon$  is the vector of  $\epsilon_{ij}$  corresponding to each pair of objects. By construction,

$$\mathbf{s}_n \sim MVN(\theta \mathbf{1}_n, \boldsymbol{\Sigma}_{n \times n}), \text{ where } \boldsymbol{\Sigma}_{n \times n} = \mathbf{P}\mathbf{P}^t \sigma_a^2 + \mathbf{I}_n \sigma_e^2. \quad (53)$$

Armstrong et al. (2017) show that  $\Sigma_{n \times n}$  has three different eigenvalues

$$\begin{aligned}\lambda_1 &= 2(N-1)\sigma_a^2 + \sigma_e; \\ \lambda_2 &= (N-2)\sigma_a^2 + \sigma_e^2 \\ \lambda_3 &= \sigma_e^2\end{aligned}\tag{54}$$

with multiplicity 1,  $N-1$ , and  $n-N$  respectively. Armstrong et al. (2017) also show that

$$\begin{aligned}|\Sigma_{n \times n}| &= (2(n-1)\sigma_a^2 + \sigma_e^2) ((n-2)\sigma_a^2 + \sigma_e^2)^{(n-1)} (\sigma_e^2)^{N-n} \\ \Sigma_{n \times n}^{-1} &= \frac{\mathbf{v}_1 \mathbf{v}_1^t}{\lambda_1} + \sum_{k=2}^n \frac{\mathbf{v}_k \mathbf{v}_k^t}{\lambda_2} + \sum_{k=n+1}^N \frac{\mathbf{v}_k \mathbf{v}_k^t}{\lambda_3}\end{aligned}\tag{55}$$

where  $\mathbf{v}_1 = \frac{1_n}{\sqrt{n}}$  and  $\mathbf{v}_k$  are eigenvectors orthogonal to  $\mathbf{v}_1$ . Importantly, Armstrong et al. (2017) note that

$$\begin{aligned}\sum_{k=2}^N \mathbf{v}_k \mathbf{v}_k^t &= \frac{(N-1)^2}{N-2} \left( \frac{1}{N-1} \mathbf{P} - \frac{1}{n} \mathbf{1}_n \mathbf{1}_n^t \right) \left( \frac{1}{N-1} \mathbf{P}^t - \frac{1}{n} \mathbf{1}_N \mathbf{1}_n^t \right) \\ \sum_{k=N+1}^n \mathbf{v}_k \mathbf{v}_k^t &= \mathbf{I}_n - \mathbf{v}_1 \mathbf{v}_1^t - \sum_{k=2}^N \mathbf{v}_k \mathbf{v}_k^t\end{aligned}\tag{56}$$

Using these results, Armstrong et al. (2017) show that the likelihood function,  $\mathcal{L}(\theta, \sigma_a^2, \sigma_e^2 | \mathbf{s}_n)$ , can be rewritten as an independent sum of squares

$$\begin{aligned}-2 \mathcal{L}(\theta, \sigma_a^2, \sigma_e^2 | \mathbf{s}_n) &= \log(\lambda_1) + (N-1) \log(\lambda_2) + (n-N) \log(\lambda_3) + n \log(2\pi) \\ &+ \frac{n(\bar{s}_n - \theta)^2}{\lambda_1} + \frac{SS_a}{\lambda_2} + \frac{SS_e}{\lambda_3}.\end{aligned}\tag{57}$$

where  $\bar{s}_n$  is the average of the elements in  $\mathbf{s}_n$ , and

$$\begin{aligned}SS_a &= \frac{(N-1)^2}{N-2} \sum_{i=1}^N (\bar{s}_n^{(i)} - \bar{s}_n)^2, \\ SS_e &= \mathbf{s}_n^t (\mathbf{I}_n - \mathbf{v}_1 \mathbf{v}_1^t) \mathbf{s}_n - SS_a,\end{aligned}\tag{58}$$

where  $\bar{s}_n^{(i)}$  is the average of the elements in  $\mathbf{s}_n$  involving object  $i$ .

Finally, Armstrong et al. (2017) show that closed-form solution estimates for the parameters of the model exist and can be derived from Table 2 to obtain

$$\begin{aligned}\hat{\theta} &= \bar{s} \\ \hat{\sigma}_a^2 &= \frac{MS_a - MS_e}{N-2} \\ \hat{\sigma}_e^2 &= MS_e.\end{aligned}\tag{59}$$

Table 2: ANOVA table for the model  $\mathbf{s}_n \sim MVN(\theta \mathbf{1}_n, \mathbf{\Sigma}_{n \times n})$

<i>Source</i>	<i>df</i>	<i>SS</i>	<i>MS</i>	<i>E(MS)</i>
A	$N - 1$	$SS_a$	$\frac{SS_a}{(N-1)}$	$(N - 2)\sigma_a^2 + \sigma_e^2$
Error	$n - N$	$SS_e$	$\frac{SS_e}{(n-N)}$	$\sigma_e^2$
Total	$n - 1$	$SS_t$	$\frac{SS_t}{(n-1)}$	

At this point, we simply note that we presented the results obtained by Armstrong et al. (2017) for a set of  $N$  objects known to come from a single source and that it is trivial to scale these results for a vector containing the pairwise scores resulting from the cross-comparisons of  $N + M$  objects, if they are assumed to originate from the same source.

## Appendix B: Multivariate normality of scores used in the worked example

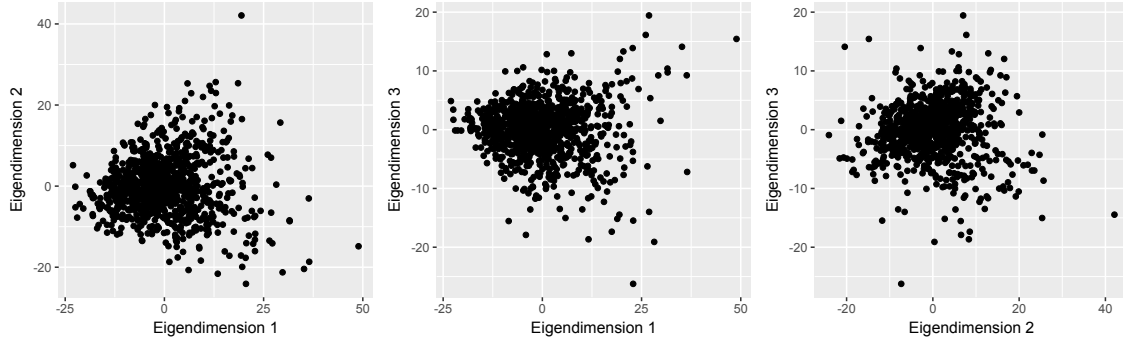


Figure 51: Projection of 3-dimensional vectors of scores obtained from 1,000 triplets of objects from a single source in the space defined by the spectral decomposition of their covariance matrix.

To examine whether the scores considered in this paper satisfy the assumption of multivariate normality of the score model proposed by Armstrong et al. (2017), we simulated 1000 triplicates of spectra from a single source. By expressing the original 3-dimensional vectors of scores as a function of the space defined by the eigenvectors of their sample covariance matrix, we can observe the marginal distributions of the score vectors along orthogonal axes. Figure 51 shows that the data is essentially spherical in the eigenspace and that our assumption of normality is mostly satisfied. The planned optimisation of the metric will enable to further improve the multivariate normality of the distribution of the data.